Full Paper

Wiley Online Library

ELECTROANALYSIS

DOI: 10.1002/elan.202000008

Porous Molybdenum Carbide Nanostructured Catalyst toward Highly Sensitive Biomimetic Sensing of H_2O_2

Juan Li[+],[a, d] Chun Tang[+],[a, d] Taotao Liang,[a, d] Chuyue Tang,[a, d] Xiaohui Lv,[a, d] Kanglai Tang,*[e] and Chang Ming Li*[a, b, c, d]

Abstract: There are great challenges to fabricate a highly selective and sensitive enzyme-free biomimetic sensor. Herein for the first time a unique nanostructure of porous molybdenum carbide impregnated in N-doped carbon (p-Mo_2C/NC) is synthesized by using SiO_2 nanocrystals-templating method and is further used as an enzyme-free electrochemical biosensor toward highly selective, sensitive detection of H_2O_2, of which the limit of detection, dynamic detection range and sensitivity accomplish as 0.22 μM, 0.05–4.5 mM and 577.14 $\mu A\,mM^{-1}\,cm^{-2}$, respectively, and are much superior to the non-porous molybdenum carbide impregnated in N-doped carbon (Mo_2C/NC). The sensor is also used to monitor H_2O_2 released from A549 living cells. This work holds a great promise to be used to monitor the presence of H_2O_2 in biological research while offering an important knowledge to design a highly selective and sensitive biomimetic sensor by synthesizing a porous catalyst to greatly improve the reaction surface area rather than conventionally only relying on dispersing the catalyst material into porous carbon substrate.

Keywords: Hydrogen peroxide · Molybdenum carbide · Electrochemical · Biomimetic sensing · Living cells

1 Introduction

Hydrogen peroxide (H_2O_2), a reactive oxygen species (ROS) plays an essential role in organisms, which is produced by oxidase enzymes in mitochondria [1–4], and can freely diffuse onto the cell membrane [5]. The toxicity of H_2O_2 is low, but its overexpression can cause irreversible damage of nucleic acid, unsaturated fatty acid, lipid peroxidation of cell membrane and other harmful biological processes. Excessive H_2O_2 may also lead to aging and some fatal diseases, including myocardial infarct, cardiovascular diseases, Parkinson's disease, cancers and Alzheimer's disease [6–9]. It is also employed in chemical synthesis, fuel cells, foods, pharmaceutical and environmental fields, etc. [10–14]. However, H_2O_2 is easy to decompose and has extremely low concentration in biological systems. Thus, it is of importance to fast and selective detection of H_2O_2 with accuracy and reliability. Various techniques have been reported to detect H_2O_2 including colorimetry [15], fluorescence [16], photochemistry [17] and electrochemical methods [18–20], among which enzymatic electrochemical H_2O_2 sensors are often used due to their high specificity, simplicity and sensitivity. In particular, electrochemical enzymatic glucose sensors for detections of glucose in blood are very popular in clinic diagnosis worldwide. However, these sensors have shortcomings of high cost, easy loss of bioactivity, short shelf-life and complicated preparation process. Thus, enzyme-free electrochemical sensors, namely biomimetic sensors are intensively investigated to overcome the shortcomings of the enzyme ones [21], of which the selectivity often relies on some transition metal ions such as $Fe^{2+/3+}$, $Cu^{1+/2+}$ and $Mn^{2+/3+}$ to catalyze the oxidation or reduction of the target biomolecule against many interferences existing in biological system, while the sensitivity can be promoted by a large reaction surface area or/and highly concentrated reaction-active centers. Although advances of the biomimetic sensors have been made, it still cannot completely replace the enzymatic ones in clinic diagnosis due to their relatively poorer selectivity and lower sensitivity. In addition, currently the most reported non-enzymatic electrochemical sensors mainly employ precious metals as the catalysts, among which platinum based materials show excellent performance in detection of H_2O_2 [22], but they are not cheap, abundant and sustainable. Hence, there is great room to further develop an inexpensive, highly

[a] J. Li,[+] C. Tang,[+] T. Liang, C. Tang, X. Lv, C. M. Li
Institute for Clean Energy and Advanced Materials, School of Materials and Energy, Southwest University, Chongqing 400715, China
E-mail: ecmli@swu.edu.cn
[b] C. M. Li
Institute of Materials Science and Devices, Suzhou University of Science and Technology, Suzhou 215011, China
[c] C. M. Li
Institute of Advanced Cross-field Science and College of Life Science, Qingdao University, Qingdao 200671, China
[d] J. Li,[+] C. Tang,[+] T. Liang, C. Tang, X. Lv, C. M. Li
Chongqing Key Laboratory for Advanced Materials and Technologies of Clean Energies, Chongqing 400715, China
[e] K. Tang
Chongqing Sports Medicine Center, Department of Orthopedic Surgery, Southwest Hospital, The Third Military Medical University, Chongqing 400038, China
E-mail: tangkanglai@hotmail.com
[+] Equal contributors

Supporting information for this article is available on the WWW under https://doi.org/10.1002/elan.202000008

selective and more sensitive non-noble-metal-based enzyme-free electrochemical H_2O_2 sensors [19].

The much inexpensive transition metals such as molybdenum, tungsten and cobalt possess good electrocatalytic activity [23] and could be used to fabricate enzyme-free sensors. In particular, it is known that molybdenum (Mo) exists in the brain [24], and should be very biocompatible. There are many reports on MoS_2 based materials for H_2O_2 detection. Nevertheless, S element is harmful for health. At present, molybdenum carbide (Mo_2C) has rarely been reported to detect H_2O_2. Further, Mo_2C has long been considered as an effective platinum-free catalyst and introduction of carbon into the transition metal lattice results in expansion of the lattice constant [25]. Doping various elements into carbon nanomaterials could greatly improve their electrocatalytic performance including catalytic activity [26], surface adsorption/desorption preparties and electronic structures [27–28]. Besides, investigations by the use of density functional theory (DFT) reveal that the hybridization of metal d orbital with carbon s orbital as well as p orbital widens the structure of d band and has the characteristics similar to platinum d band [25]. In this work, we consider using Mo_2C as the catalyst to offer the specificity for the first time toward detection of H_2O_2. We further use a SiO_2 template to produce Mo_2C–SiO_2 nanocomposite, followed by etching out SiO_2 to produce a porous Mo_2C (p-Mo_2C), which renders a porous catalyst for high reaction surface area and then dispersing to nitrogen-doped carbon (p-Mo_2C/NC) and is different from the conventional approach, in which the sensor catalyst materials mainly rely on dispersing into a porous carbon substrate for large reaction surface area. The prepared sample was evaluated by SEM, TEM, XRD, Raman, XPS and BET to confirm the physical and chemical properties of p-Mo_2C. The electrochemical measurements present that the p-Mo_2C sensor without the use of enzyme has high sensitivity, high selectivity and excellent stability toward detection of H_2O_2. In addition, the electrochemical sensor was used to detect H_2O_2 released by human lung adenocarcinoma cells (A549), indicating that p-Mo_2C/NC biomimetic sensor can be used for applications in biological research to monitor H_2O_2 released in various biological researches. The preparation and detection of H_2O_2 is schematically shown in Scheme 1.

2 Experimental Sections

2.1 Materials

Sodium hydroxide (NaOH), ammonium heptamolybdate tetrahydrate ($(NH_4)_6Mo_7O_{24}$), melamine ($C_3N_6H_6$), SiO_2, KCl and KOH were purchased from Shanghai Aladdin Bio-Sciences Co., Ltd. Glycine, $CaCl_2$, uric acid (UA), ascorbic acid (AA), dopamine (DA), glucose, 30 % H_2O_2 were all obtained from Sigma Aldrich. Phosphate buffered solution

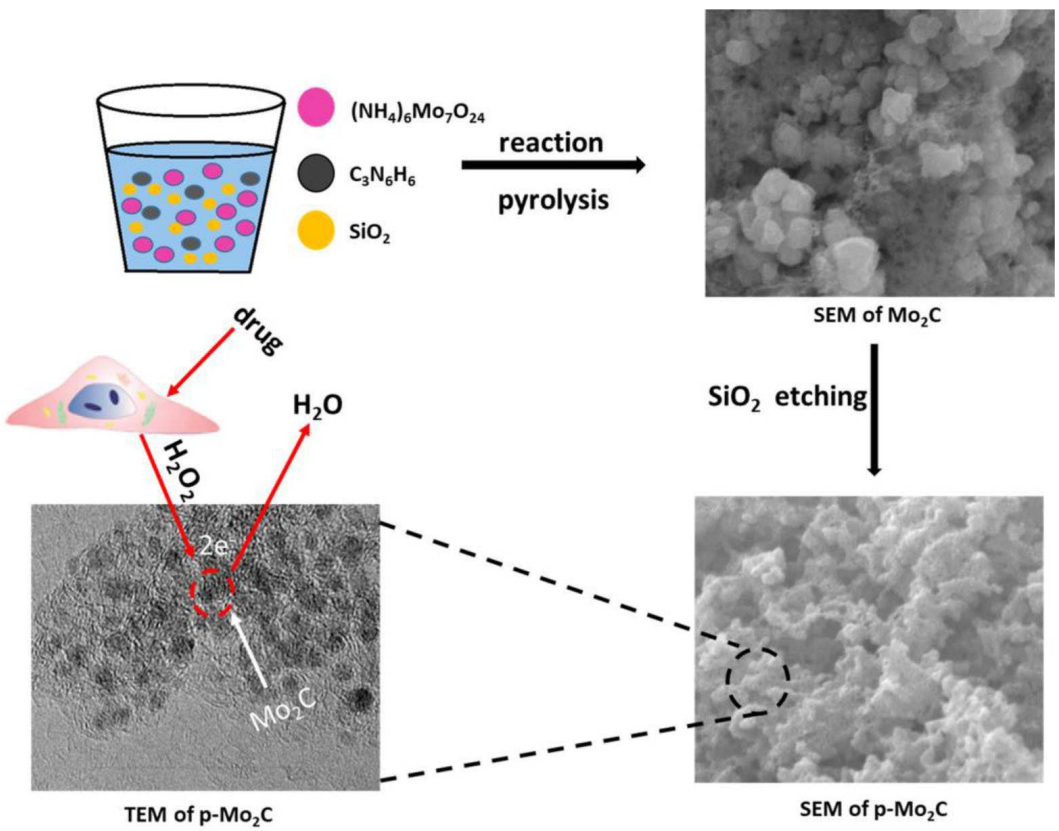

Scheme 1. synthesis process of porous molybdenum carbide embedded in N-doped carbon (p-Mo_2C/NC) and monitoring H_2O_2 released from A549 cell.

(PBS), Iron (III) chloride hexahydrate ($FeCl_3.6H_2O$), potassium ferricyanide [$K_3Fe(CN)_6$], Nafion were ordered from Chongqing Co. All reagents and solvents were analytic grade and used without further purification. The deionized water used in all experiments was produced by Q-Grad®1 system, Millipore Corporation.

2.2 Synthesis of p-Mo_2C/NC

In preparation 1000 mg $(NH_4)_6Mo_7O_{24}$, 500 mg melamine and 1000 mg SiO_2 were dissolved in deionized water by physical stirring for one hour to form a homogeneous solution, followed by evaporating overnight at 80 °C to form a uniform white powder. Then the powder was annealed at 900 °C inert atmosphere for 2 hours. Finally, the as prepared annealed sample was placed in hydrofluoric acid (HF) solution to etch out SiO_2 for producing p-Mo_2C/NC with one pot chemistry. The nano-porous Mo_2C/NC was synthesized as the same way of p-Mo_2C/NC but without adding SiO_2 and the following etching step.

2.3 Fabrication of p-Mo_2C/NC Electrodes

The glassy carbon electrode (GCE, 3 mm diameter) was polished to have a mirror-like surface using 0.05 μm alumina slurry followed by thoroughly sonicating in both distilled water and 75 % ethanol for twice to remove adsorbed alumina particles before drying in N_2 flow. The optimal concentration of p-Mo_2C/NC aqueous solution (8 μL, 2.5 mg mL^{-1}) as described in Supporting Information Figure S1 was dropped onto the cleaned GCE and dried under infrared lamp to obtain p-Mo_2C/NC/GCE. 0.5 % Nafion solution was then deposited on the top of the prepared p-Mo_2C/NC/GCE. For comparison, Mo_2C/NC electrode was also made with the same procedure. These electrodes were denoted as p-Mo_2C/NC and Mo_2C/NC, respectively.

2.4 Material Characterization

The as-prepared materials were characterized by Scanning Electron Microscopy (SEM, JSM-6700F) and Transmission Scanning Electron Microscopy (TEM, JEM-2100F), respectively. Nitrogen adsorption/desorption were examined by Bruneian-Emmett-Teller (BET) Surface Area & Pore Size Analyzer. The crystalline phase of the composite was examined by X-ray diffraction (XRD, XRD-7000) with Cu $K_{\alpha 1}$ radiation ($\lambda = 1.5406$ Å). The surface properties of the materials were measured by X-ray photoelectron spectroscopy (XPS, Escalab 250xi, Thermo Scientific). Raman patterns were recorded on Renishaw Invia Raman spectrometer equipped with a 532 nm laser source.

2.5 Electrochemical Measurements

All Electrochemical measurements were performed with CHI 660D electrochemical workstation (ChenHua, Shanghai, China) associated with a three-electrode system. The pre-modified GCE was utilized as the working electrode, while a platinum and Ag/AgCl electrode in saturated KCl solution were employed as auxiliary and reference electrode, respectively. The buffer solution was bubbled with pure nitrogen for at least 20 min and then maintained nitrogen atmosphere environment during measurements. All electrochemical measurements were conducted in 0.01 M phosphate buffer electrolyte with pH 7.4 at 25 °C.

2.6 Cell Culture and Real-time H_2O_2 Detection

Fetal bovine serum, penicillin and streptomycin were added into high-glucose Dulbecco's modified Eagle medium (DMEM) to have concentrations of 10 % (v/v), 100 U mL^{-1} and 100 mg mL^{-1}, respectively and was placed in a humidified incubator (95 % air with 5 % CO_2) at 37 °C to grow human lung adenocarcinoma cells (A549 cells) to ca. 90 % fusion. Then the cells were collected with centrifugating at 1000 rpm for 3 minutes and then washed three times by PBS (10 mM, pH 7.4). Figure S2 presents the picture of cells in PBS, in which the cell number was ~10^6 cells in 2 ml solution determined by a hemocytometer. Chronoamperometry was performed to real-time detect H_2O_2 released from living cells by injecting 0.1 M NaOH into the tested cell system. A cell sample with 3500 U mL^{-1} catalase was employed as the control.

3 Results and Discussion

The microstructure of p-Mo_2C/NC was characterized by SEM (Figure 1a) and TEM (Figure 1b and c). Figure 1a displays that the as-prepared p-Mo_2C/NC has a porous faveolated structure with massive hierarchical pores derived

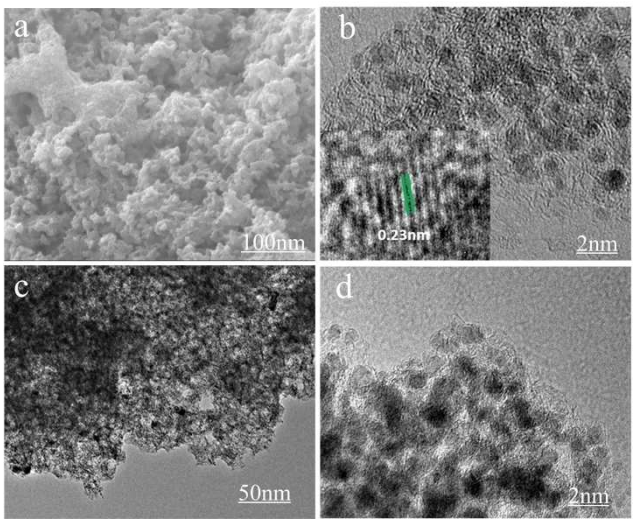

Fig. 1. (a) SEM (b) TEM and (c) HRTEM images of p-Mo_2C/NC (d) HRTEM images of Mo_2C/NC.

from the residual spaces after removal of SiO_2 nanospheres templates. The pore structure should be formed partially by gas bubbling during the pyrolysis process. A closer TEM examination of the p-Mo_2C/NC clearly reveals that many ultrafine nanoparticles are well dispersed on the amorphous carbon (Figure 1b). A small diameter of ~2 nm in an average size for Mo_2C can be observed from Figure 1c, a High resolution TEM image (HRTEM). Besides, it lucidly exhibits a set of lattice fringes with an interplanar space of 0.23 nm, which corresponds to (111) planes of hexagonal Mo_2C, further confirming that the phase composition of these nanoparticles is Mo_2C. While without using SiO_2 template method, Mo_2C/NC nanocomposite tends to be agglomerate (Figure S3 and Figure 1d) with decreased exposed active surface. These results clearly disclose that the presence of SiO_2 during the heat treatment process can efficiently change Mo_2C/NC into p-Mo_2C/NC.

The structure and composition of p-Mo_2C/NC were further examined by X-ray diffraction (Figure 2a). The broad peak near 26° with relatively low intensities can be assigned to amorphous carbon [29–30] derived from melamine. The other peaks located at 2θ of 39.4°, 52.1°, 61.5°and 75.5° can be ascribed to (101), (102), (110) and (112) faces of hexagonal Mo_2C (JCPDS No. 35-0787), respectively. The full width at half maxima (FWHM) of p-Mo_2C/NC is broad, indicating the ultrasmall crystallite size of Mo_2C or Mo_2C coated with amorphous carbon [31–33]. Raman spectrum for p-Mo_2C/NC in Figure 2b exhibits fingerprint bands characteristic of Mo_2C at 654, 810, and 981 cm^{-1}, as well as broad D and G bands between 1300 and 1600 cm^{-1} for graphitic carbon. The intensity ratio between D and G bands (I_D/I_G) was found to be 1.2, which suggests the presence of significant structural defects within p-Mo_2C/NC, presumably stemming from the existence of a large amount of N dopants in the carbon layer. The BET surface areas and pore size distributions of p-Mo_2C/NC and Mo_2C/NC were examined by nitrogen adsorption-desorption isotherm measurement (Figure 2c), from which the calculated specific area of p-Mo_2C/NC and Mo_2C/NC are 142.6 and 18.3 $m^2 g^{-1}$, respectively, clearly indicating that p-Mo_2C/N has almost 8 times larger specific surface area than Mo_2C/NC, which is obviously caused by the etching out of SiO_2 template. Figure 2d shows the pore size distribution of p-Mo_2C/NC mainly concentrates around 15 nm but with a wide range of larger pore sizes distributions, while Mo_2C/NC is much less porous with a very little distribution of pores around 2 nm, which could be considered a kind of surface roughness.

X-ray photoelectron spectroscopy (XPS) analysis of p-Mo_2C/NC were further carried out to examine their valence states and compositions. As observed from Figure 3a, the survey spectrum confirms the presence of Mo, C, O and N elements, of which O element is very likely from the self-oxidation of material surface. Figure 3b shows the high-resolution of Mo 3d spectrum, which can be de-convoluted into four Mo 3d doublets by peak fitting, corresponding to Mo^0 (228.2, 228.7 ev), Mo^{3+} (229.4, 231.3 ev), Mo^{4+} (231.9, 232.5 ev) and Mo^{6+} (233.1, 235.2 ev) oxidation states of Mo. Mo^0 originates from the Mo–Mo bond in molybdenum carbide, and the low

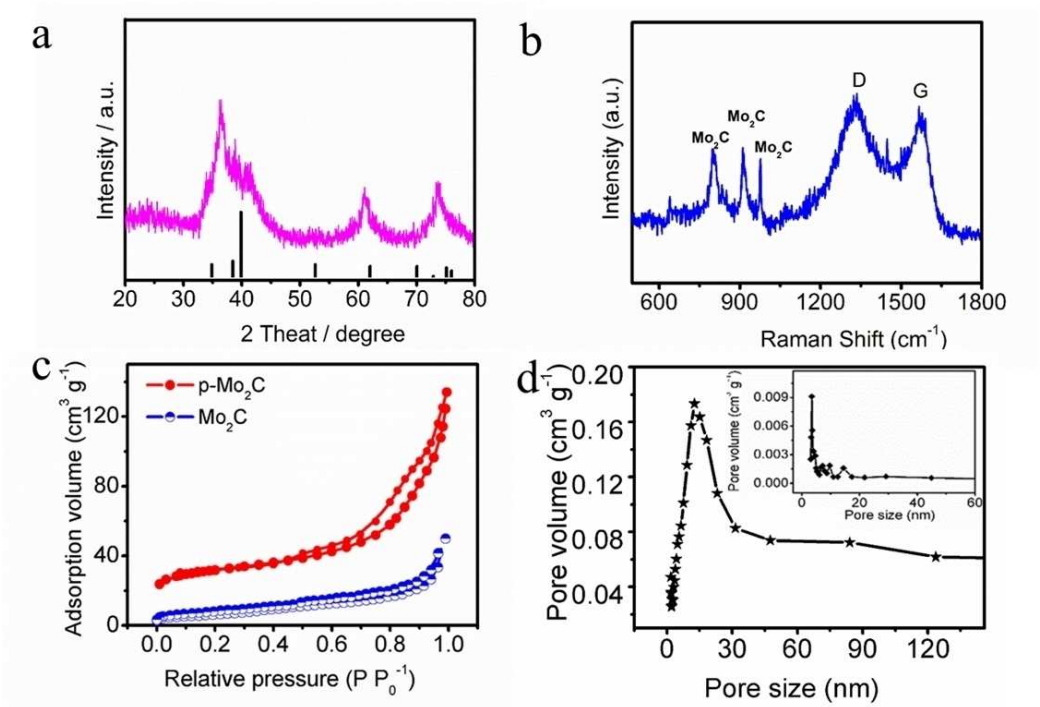

Fig. 2. (a) XRD, (b) Rama images of p-Mo_2C/NC (c) Nitrogen adsorption-desorption isotherms of p-Mo_2C/NC and Mo_2C/NC (d) BJH pore size distributions of p-Mo_2C/NC (inset: Mo_2C/NC).

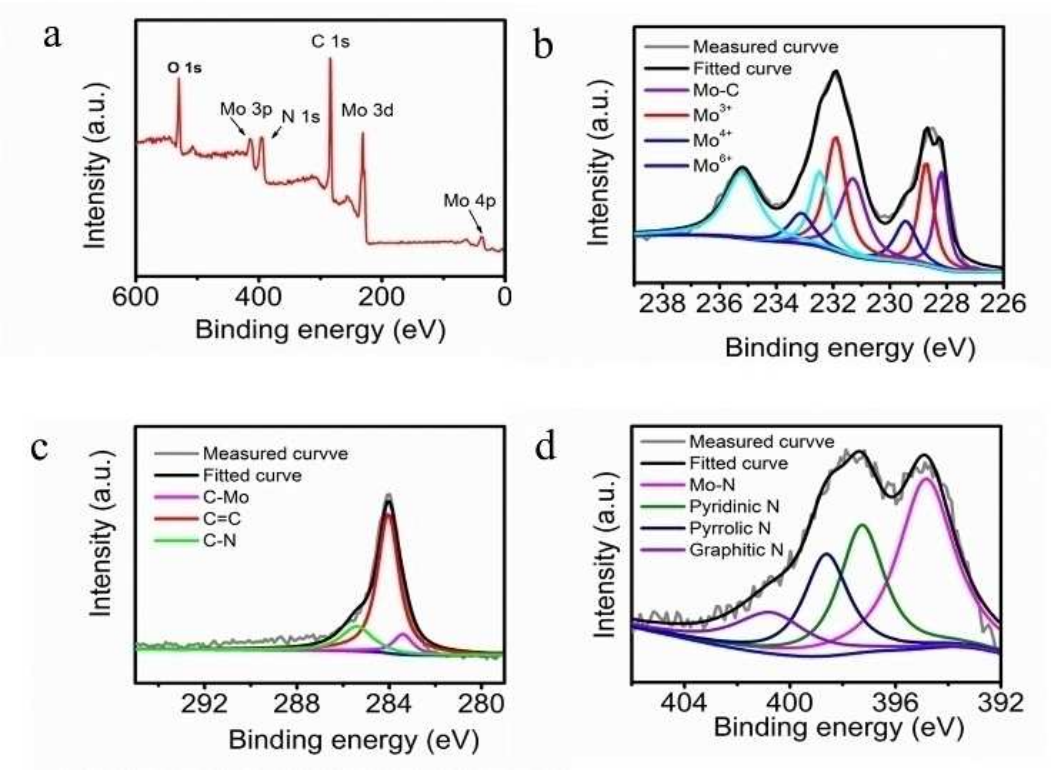

Fig. 3. (a) XPS survey spectrum for p-Mo_2C/NC. XPS spectra in the (b) Mo 3d, (c) C1s, and (d) N 1s regions.

oxidation states of Mo^{3+} may come from Mo–Mo and Mo–C bonds in molybdenum carbide. The oxidation state of $Mo^{4+/6+}$ is also observed, which probably originates from the slight surface oxidation (MoO_2 and MoO_3) of Mo_2C [34–35]. The XPS spectrum of C1s can be deconvoluted into carbonic bonded carbon, proving the formation of molybdenum carbides. (Figure 3c). N1s of high-resolution XPS spectra (Figure 3d) is also collected to reveal the electronic status of dopants in graphene.

Figure 4a shows CV curves of the p-Mo_2C/NC nanocomposite in the presence and absence of 3 mM H_2O_2 in 0.01 M PBS, respectively. Clearly, it has no electrochemical response at the absence of H_2O_2 (black), while a well-defined reduction peak appears at −0.5v during the cathodic scanning on p-Mo_2C/NC electrode when 3 mM H_2O_2 exists (red). It reveals that p-Mo_2C/NC nanocomposite has excellent catalytic activity toward H_2O_2 reduction.

In contrasts, Cyclic Voltammetry (CV) curves of the plain and Mo_2C/NC electrodes were also measured in 0.01 M PBS containing 3 mM H_2O_2. Results in Figure 4b illustrate that the plain electrode (black) has no apparent current change in comparison to the well-defined reduction peak of p-Mo_2C/NC (red), while the shape of the Mo_2C/NC electrode is similar to that of p-Mo_2C/NC electrode, but the peak current is only one third as large as that of the p-Mo_2C/NC electrode. In addition, the reduction peak potential of p-Mo_2C/NC is more positive than that of Mo_2C/NC. The larger peak current and more positive peak potential of p-Mo_2C/NC indicate that the former has much larger reaction surface area and higher electrocatalytic activity than Mo_2C/NC, respectively.

The CV curves of the p-Mo_2C/NC electrode in 3 mM H_2O_2 were measured with 5 to 100 mvs^{-1}. Figure 4c displays that the reduction peak potential negatively shifts with the increased scan rates, symboling an irreversibility nature of H_2O_2 reduction. Further, the good linear relation of peak current (I_p) against square root of scan rate ($v^{1/2}$) in Figure 4c specifies that H_2O_2 reduction is a diffusion controlled electrode process [42]. Additionally, the CV and chronoamperomtric measurements were used to evaluate the sensing property of p-Mo_2C/NC. Figure S4 exhibits the CV measured with 50 mvs^{-1} on p-Mo_2C/NC for different concentrations of H_2O_2 in 0.01 M PBS. Result specifies that the reduction peak current increases with the increased H_2O_2 concentration, and illustrates a good linear relation of i_p versus H_2O_2 concentration with a high correlation of $R^2 = 0.995$ (Inset of Figure S4).

Figure 5a shows a typical steady-state current-time (i-t) response plot with continuous addition of the different H_2O_2 concentration into the stirring PBS solution approximately every 50s at the optimal potential of −0.65v (Figure S5) using the chronoamperomtric method. Figure 5a also displays a clear stepwise increase of the current responses immediately after injection of H_2O_2. A curve of current versus H_2O_2 concentration over a range of 50 μM to 4500 μM (Figure 5b) could be derived from Figure 5a. In addition, the sensor sensitivity and limit of detection can be calculated from the calibration curve

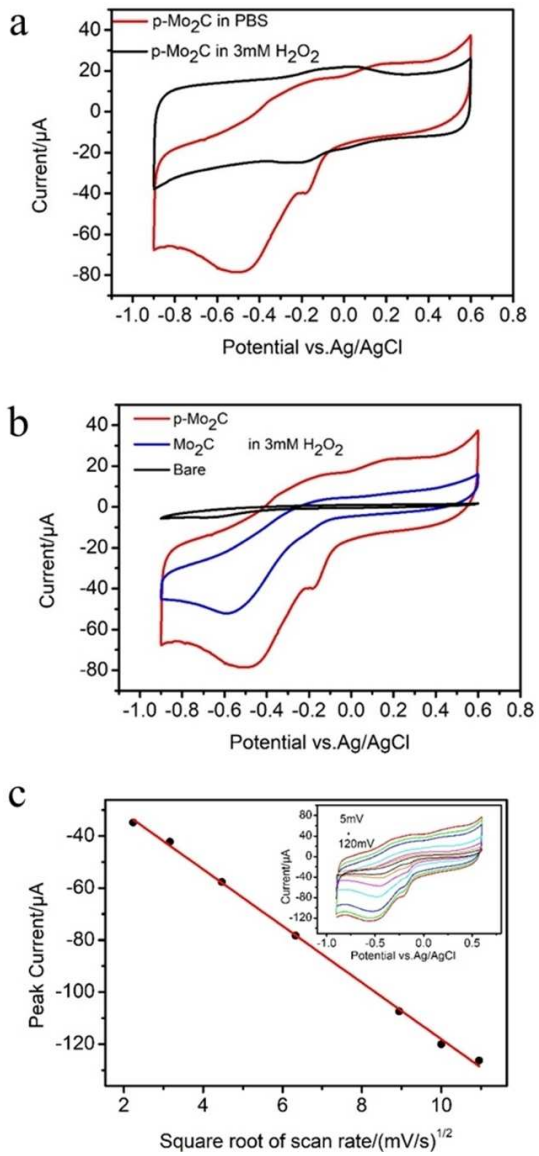

Fig. 4. (a) CVs of the p-Mo_2C/NC Modified electrode in the presence and absence of 3 mM H_2O_2, (b) CVs of different modified electrodes in the presence of 3 mM H_2O_2. (c) Relation of peak currents against scan rates plotted from the CVs measured at p-Mo_2C/NC. Inset: different scan rates of p-Mo_2C/NC modified electrode in 3 mM H_2O_2 at a scan rate of 5–120 mv s^{-1}.

(Figure 5b). It is known that the sensitivity can be expressed as sensitivity = slope/electrode surface area and limit of detection = $3S_b$/slop [43], in which S_b is the standard deviation of the lowest signal. The p-Mo_2C/NC sensor demonstrates remarkable sensitivity (577.14 μA mM^{-1} cm^{-2}) and low limit of detection (LOD) (0.22 μM), which offers a comparable sensitivity among recently reported noble metal-free Mo-based H_2O_2 sensors as in Table 1, even higher than some noble metal-based H_2O_2 sensors.

Considering many other electrochemically reactive species may exist in biological fluids, such as AA, UA, DA, glucose, glycine, Ca^{2+}, K^+, interference effects of these reactive species were evaluated for p-Mo_2C/NC sensor selectivity. Figure 5c shows the amperometric responses of p-Mo_2C/NC modified electrode to successive injected 1 mM H_2O_2, 50-fold excess concentration of AA, UA, DA, glucose, Glycine, Ca^{2+}, K^+ and 1 mM H_2O_2, respectively, indicating the interferences from AA, UA, DA, glucose, Ca^{2+} and K^+ are almost negligible. As we know, the endogenous levels of AA, glucose and UA in blood is ca. 0.125 mM, 4.4–6.6 mM, and 0.33 mM, respectively [44–45], which concentrations are far small than what we use in the Interference experiment. It can be concluded that the p-Mo_2C/NC biomimetic sensor renders very good selectivity toward detection of H_2O_2.

The stability of the p-Mo_2C/NC sensor was tested for a month to discontinuously detect H_2O_2, in which the sensor was stored at 4 °C and was used to detect H_2O_2 every six days by adding 3 mM H_2O_2. The measured current relative standard deviation (RSD) is lower than 1.3 % (Figure S6). The sensor reproducibility was tested by using six different p-Mo_2C/NC sensors to undergo the evaluations discussed above in parallel. The results in Figure S7 show that the RSD for sensor-to-sensor reproducibility is less than 0.8 %, demonstrating good reproducibility toward detection of H_2O_2.

Human lung adenocarcinoma cell (A549) was used to assess the applications ability of the constructed sensor. Experiments were designed to certify that the p-Mo_2C/NC sensor can specifically detect H_2O_2 released from A549 cell. Three solutions were prepared: 0.01 M PBS, 0.01 M PBS + A549 + catalase and 0.01 M PBS + A549. It is very interesting to observe that only current response is measured in 0.01 M PBS + A549 when NaOH is added to treat the three solutions. The instant current response (curve a, Figure 5d) should be attributed to the fast cellular secretion of H_2O_2 upon the stimulation of NaOH. However, in contrast, the p-Mo_2C/NC sensor in both 0.01 M PBS and 0.01 M PBS + A549 + catalase solutions with NaOH treatment has no current response toward H_2O_2 (Curve b and c, respectively in Figure 5d). This can be reasonably explained. It is known that A549 cell releases H_2O_2 when NaOH is added in to treat the cells[46], while A549 cells co-exist with catalase, NaOH treatment cannot stimulate the H_2O_2 release since catalase can specifically degrade H_2O_2 [46–47]. These results unquestionably testify that the developed biomimetic sensor can be used in biological research for H_2O_2 detection.

As discussed above, the challenges of a noble metal-free biomimetic sensor without the enzyme catalyst come from its selectivity and sensitivity. This work vividly shows us the enhancement mechanism and design principle for a biomimetic sensor as schematically shown in Figure 6, in which Mo_2C serves as a reaction center to specifically catalyze the H_2O_2 reduction for good selectivity, while the porous catalyst structure rather than only catalyst particles-dispersed in a porous carbon support substrate offers much larger reaction surface area and fast mass transport paths for high sensitivity.

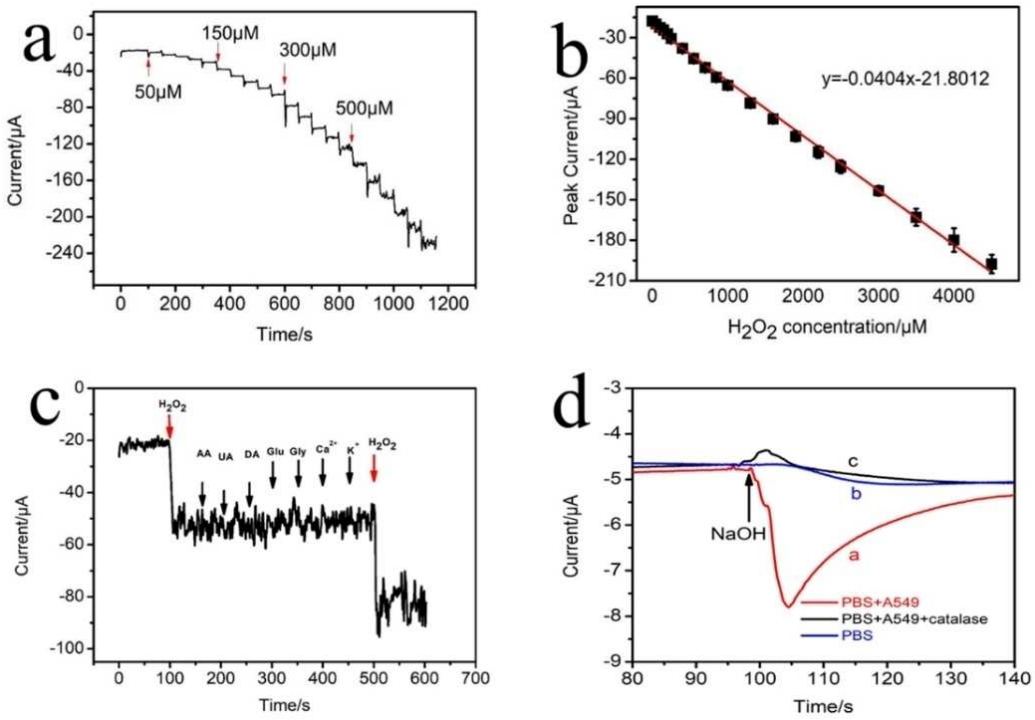

Fig. 5. (a) Typical Amperometric curve recorded at −0.65 v in 0.01 M PBS (pH = 7.4) for p-Mo_2C/NC nanocomposite modified electrode successively injected designated amounts of H_2O_2 each time. (b) Calibration plot of the response current vs. the H_2O_2 concentration. (c) Amperometric response of the p-Mo_2C/NC nanocomposite modified electrode to the sequential addition of 1 mM H_2O_2, 50-fold excess concentration of AA, UA, DA, glucose, Glycine, Ca^{2+}, K^+ and 1mMH_2O_2 respectively.(d) Amperometric responses of the p-Mo_2C/NC modified GCE with the addition of NAOH at −0.65 v in (a) PBS containing ~1×10^6 A549 cells, (b) PBS (c) PBS containing 1×10^6 A549 cells and 3500 U/mL catalases.

Table 1. Comparative table of analytical performance of Mo-based H_2O_2 electrochemical sensors.

Catalyst	Linear range (μM)	Sensitivity ($\mu A\,cm^{-2}\,mM^{-1}$)	LOD (μM)	Ref.
MoS_2/C_NNWs	2–500	13.19	0.73	[36]
CAT/MoS_2–Au/chitosan GCE	0.5–200	187.4	0.1	[5]
(2D)α-MoO_3	0.4–57600	168.72	0.076	[6]
O–MoS_2/graphene	250–1000	269.7	0.12	[10]
MoS/rGO	50–20000	33.2	2	[37]
AgNPs/MoS_2	25–135200	54.5	3.5	[38]
Au–Pd/MoS_2/GCE	0.8–10000	184.9	0.16	[39]
Alpha-MoO_3/GO/GCE	0.92–2460	391.39	0.31	[24]
Mb@$MnMoSe_2$/GCE	0.09–60	222.78	0.004	[40]
MoS_2/CC	5–3000	5.3	1	[41]
p-Mo_2C/NC	50–4500	577.14	0.22	This work

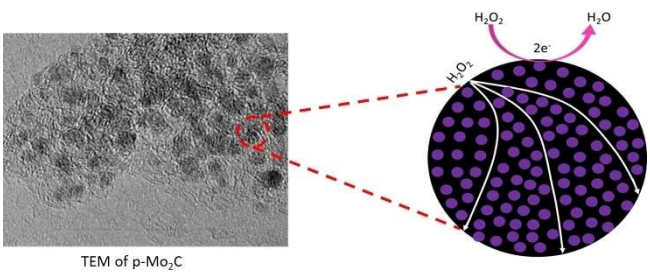

Fig. 6. Catalytic mechanisms of p-Mo_2C.

4 Conclusion

In summary, a porous Mo_2C catalyst was prepared by one-step pyrolysis of $(NH_4)_6Mo_7O_2$, melamine and SiO_2 to fabricate a sensitive, selective and stable p-Mo_2C/NC sensor toward H_2O_2 detection for the first time. The H_2O_2 sensor displays a high sensitivity (577.14 $\mu A\,mM^{-1}\,cm^{-2}$), good selectivity and excellent stability/reproducibility. The excellent biomimetic performance can be attributed to the porous Mo_2C catalyst rather than conventionally relying on only catalyst dispersing in a porous substrate for a large reaction surface area. This work holds great

promise for a biomimetic sensor to be used in biological research, while offer scientific lights on how designing high-performance enzyme-free biomimetic sensors from both chemistry and physics.

Acknowledgements

This work is financially supported by National Critical Research Program in Sport Injury and Repair Program and Institute for Clean Energy & Advanced Materials (Southwest University, Chongqing, China), Chongqing Key Laboratory for Advanced Materials & Technologies of Clean Energies.

References

[1] J. V. Kumar, R. Karthik, S. M. Chen, V. Muthuraj, C. Karuppiah, *Sci. Rep.* **2016**, *6*, 34149.
[2] T. T. Zhang, Y. Gu, C. Li, X. Y. Yan, N. N. Lu, H. Liu, Z. Q. Zhang, H. Zhang, *ACS Appl. Mater. Interfaces* **2017**, *9*, 37991–37999.
[3] M. Asif, A. Aziz, A. Q. Dao, A. Hakeem, H. T. Wang, S. Dong, G. A. Zhang, F. Xiao, H. F. Liu, *Anal. Chim. Acta* **2015**, *898*, 34–41.
[4] B. Rezaei, N. Askarpour, M. Ghiaci, F. Niyazian, A. A. Ensafi, *Electroanalysis* **2015**, *27*, 1457–1465.
[5] Y. Shu, J. Y. Chen, Q. Xu, Z. Wei, F. P. Liu, R. Lu, S. Xu, X. Y. Hu, *J. Mater. Chem. B* **2017**, *5*, 1446–1453.
[6] Z. Wei, Z. Hai, M. K. Akbari, D. C. Qi, K. J. Xing, Q. Zhao, F. Verpoort, J. Hu, L. Hyde, S. Zhuiykov, *Sens. Actuators B* **2018**, *262*, 334–344.
[7] X. H. Shu, Y. Chen, H. Y. Yuan, S. F. Gao, D. Xiao, *Anal. Chem.* **2007**, *79*, 3695–3702.
[8] Y. B. Wei, Y. Zhang, Z. W. Liu, M. L. Guo, *Chem. Commun.* **2010**, *46*, 4472–4474.
[9] D. Pramanik, S. G. Dey, *J. Am. Chem. Soc.* **2011**, *133*, 81–87.
[10] Y. D. Xue, G. Maduraiveeran, M. Y. Wang, S. L. Zheng, Y. Zhang, W. Jin, *Talanta* **2018**, *176*, 397–405.
[11] O. S. Keen, S. Baik, K. G. Linden, D. S. Aga, N. G. Love, *Environ. Sci. Technol.* **2012**, *46*, 6222–6227.
[12] J. H. Ma, W. J. Song, C. C. Chen, W. H. Ma, J. C. Zhao, Y. L. Tang, *Environ. Sci. Technol.* **2005**, *39*, 5810–5815.
[13] C. G. Tsiafoulis, P. N. Trikalitis, M. I. Prodromidis, *Electrochem. Commun.* **2005**, *7*, 1398–1404.
[14] T. Marimuthu, M. R. Mahmoudian, S. Mohamad, Y. Alias, *Sens. Actuators B* **2014**, *202*, 1037–1043.
[15] S. Liu, J. Q. Tian, L. Wang, Y. W. Zhang, Y. L. Luo, H. Y. Li, A. M. Asiri, A. O. Al-Youbi, X. P. Sun, *ChemPlusChem* **2012**, *77*, 541–544.
[16] J. A. Royall, H. Ischiropoulos, *Arch. Biochem. Biophys.* **1993**, *302*, 348–355.
[17] J. Ju, R. Z. Zhang, W. Chen, *Sens. Actuators B* **2016**, *228*, 66–73.
[18] L. S. Xie, A. M. Asiri, X. P. Sun, *Sens. Actuators B* **2017**, *244*, 11–16.
[19] F. Y. Xie, X. Q. Cao, F. L. Qu, A. M. Asiri, X. P. Sun, *Sens. Actuators B* **2018**, *255*, 1254–1261.
[20] Q. Wang, M. Li, S. Szunerits, R. Boukherroub, *Electroanalysis* **2014**, *26*, 156–163.
[21] H. X. Dai, Y. L. Chen, X. Y. Niu, C. J. Pan, H. L. Chen, X. G. Chen, *Biosens. Bioelectron.* **2018**, *118*, 36–43.
[22] F. L. Zhou, Z. Wang, B. Xu, L. Xia, X. L. Xiong, X. P. Sun, *Mater. Res. Express* **2019**, *6*, 065055.
[23] Z. K. Kou, T. T. Wang, Y. Cai, C. Guan, Z. H. Pu, C. R. Zhu, Y. T. Hu, A. M. Elshahawy, J. Wang, S. C. Mu, *Small Methods* **2018**, *2*, 1700396.
[24] B. Li, H. Y. Song, Z. P. Deng, L. H. Huo, S. Gao, *Sens. Actuators B* **2019**, *288*, 641–648.
[25] W. F. Chen, J. T. Muckerman, E. Fujita, *Chem. Commun.* **2013**, *49*, 8896–8909.
[26] D. S. Geng, N. Ding, T. S. A. Hor, Z. L. Liu, X. L. Sun, Y. Zong, *J. Mater. Chem. A* **2015**, *3*, 1795–1810.
[27] H. T. Liu, Y. Q. Liu, D. B. Zhu, *J. Mater. Chem.* **2011**, *21*, 3335–3345.
[28] K. P. Gong, F. Du, Z. H. Xia, M. Durstock, L. M. Dai, *Science* **2009**, *323*, 760–764.
[29] W. J. Zhou, J. Zhou, Y. C. Zhou, J. Lu, K. Zhou, L. J. Yang, Z. H. Tang, L. G. Li, S. W. Chen, *Chem. Mater.* **2015**, *27*, 2026–2032.
[30] R. Wu, J. F. Zhang, Y. M. Shi, D. Liu, B. Zhang, *J. Am. Chem. Soc.* **2015**, *137*, 6983–6986.
[31] R. G. Ma, Y. Zhou, Y. F. Chen, P. X. Li, Q. Liu, J. C. Wang, *Angew. Chem. Int. Ed.* **2015**, *54*, 14723–14727.
[32] J. Deng, P. J. Ren, D. H. Deng, X. H. Bao, *Angew. Chem. Int. Ed.* **2015**, *54*, 2100–2104.
[33] W. Q. Zheng, T. P. Cotter, P. Kaghazchi, T. Jacob, B. Frank, K. Schlichte, W. Zhang, D. S. Su, F. Schuth, R. Schlogl, *J. Am. Chem. Soc.* **2013**, *135*, 3458–3464.
[34] Y. P. Liu, G. T. Yu, G. D. Li, Y. H. Sun, T. Asefa, W. Chen, X. X. Zou, *Angew. Chem. Int. Ed. Engl.* **2015**, *54*, 10752–10757.
[35] H. Yu, H. S. Fan, J. Wang, Y. Zheng, Z. F. Dai, Y. Z. Lu, J. H. Kong, X. Wang, Y. J. Kim, Q. Y. Yan, J. M. Lee, *Nanoscale* **2017**, *9*, 7260–7267.
[36] H. X. Dai, D. Chen, P. F. Cao, Y. Li, N. Wang, S. J. Sun, T. Chen, H. Y. Ma, M. Lin, *Sens. Actuators B* **2018**, *276*, 65–71.
[37] S. S. Zhang, R. J. Liu, S. W. Li, A. Dolbecq, P. Mialane, L. Suo, L. H. Bi, B. F. Zhang, T. B. Liu, C. X. Wu, L. K. Yan, Z. M. Su, G. J. Zhang, B. Keita, *J. Colloid Interface Sci.* **2018**, *514*, 507–516.
[38] Z. T. Zhao, J. Liu, W. D. Wang, J. Zhang, G. Li, J. Q. Liu, K. Lian, J. Hu, S. Zhuiykov, *Int. J. Electrochem. Sci.* **2017**, *12*, 8761–8776.
[39] X. Y. Li, X. Z. Du, *Sens. Actuators B* **2017**, *239*, 536–543.
[40] S. Ramaraj, M. Sakthivel, S. M. Chen, B. S. Lou, K. C. Ho, *ACS Appl. Mater. Interfaces* **2019**, *11*, 7862–7871.
[41] H. T. Du, X. Y. Zhang, Z. Liu, F. L. Qu, *Chem. Commun.* **2019**, *55*, 9653–9656.
[42] T. T. Liang, L. Zou, X. G. Guo, X. Q. Ma, C. Zhang, Z. Zou, Y. H. Zhang, F. X. Hu, Z. S. Lu, K. L. Tang, C. M. Li, *Adv. Funct. Mater.* **2019**, *29*, 1903026.
[43] D. M. Lin, Y. Li, P. P. Zhang, W. S. Zhang, J. W. Ding, J. F. Li, G. Wei, Z. Q. Su, *RSC Adv.* **2016**, *6*, 52739–52745.
[44] J. Wang, *Chem. Rev.* **2008**, *108*, 814–825.
[45] S. Hrapovic, Y. L. Liu, K. B. Male, J. H. T. Luong, *Anal. Chem.* **2004**, *76*, 1083–1088.
[46] C. Li, R. J. Wu, J. C. Zou, T. T. Zhang, S. F. Zhang, Z. Q. Zhang, X. Hu, Y. Q. Yan, X. M. Ling, *Biosens. Bioelectron.* **2018**, *116*, 81–83.
[47] Q. Chen, M. G. Espey, M. C. Krishna, J. B. Mitchell, C. P. Corpe, G. R. Buettner, E. Shacter, M. Levine, *Proc. Natl. Acad. Sci. USA* **2005**, *102*, 13604–13609.
[48] P. Wu, Z. W. Cai, Y. Gao, H. Zhang, C. X. Cai, *Chem. Commun.* **2011**, *47*, 11327–11329.

Received: January 4, 2020
Accepted: January 30, 2020
Published online on February 12, 2020

